Nano Research

ISSN 1998-0124 CN 11-5974/O4
https://doi.org/10.1007/s12274-022-4925-y

Research Article

Bioresponsive cisplatin crosslinked albumin hydrogel served for efficient cancer combination therapy

An Yan[1], Zherui Zhang[1,3], Jiamei Gu[1], Xiaoran Ding[1], Yongchen Chen[1], Jingjing Du[1], Shu Wei[2] (✉), Hongcheng Sun[1], Jiayun Xu[1], Shuangjiang Yu[1] (✉), and Junqiu Liu[1]

[1] *College of Material, Chemistry and Chemical Engineering, Key Laboratory of Organosilicon Chemistry and Material Technology, Ministry of Education, Hangzhou Normal University, Hangzhou 311121, China*
[2] *Jing Hengyi School of Education, Hangzhou Normal University, Hangzhou 311121, China*
[3] *College of Chemistry, State Key Laboratory of Supramolecular Structure and Materials, Jilin University, Changchun 130012, China*

Received: 16 July 2022 / **Revised:** 11 August 2022 / **Accepted:** 15 August 2022

ABSTRACT

Combination therapy is one of the potential strategies for tackling complicated tumor treatments like drug resistance. In this work, we have generated a therapeutic cisplatin-crosslinked albumin hydrogel (BC-Gel) that allows the local release of L-Buthionine-sulfoximine (BSO), cisplatin, and glucose oxidase (GOx) with distinct release kinetics. The BC-Gel with favorable biostimuli degradability and injectability could release therapeutic agents in a programmed manner within the tumor microenvironment (TME). The preferentially released BSO significantly suppressed the glutathione (GSH)-related cisplatin resistance and sensitized the tumor cells to cisplatin by inhibiting the γ-glutamylcysteine synthetase. Meanwhile, cisplatin achieved a sequential release and long-term treatment following the bioresponsive gel degradation under the combined action of chloride ions (Cl^-) and proteinase in the body. In addition, the overproduced H_2O_2 of GOx-catalyzed glucose oxidation accelerated the depletion of existed GSH within cells and further weakened the cisplatin resistance, achieving enhanced tumor treatment together with a strong cell-killing effect. The above sequential drug release strategy based on the dual GSH depletion effect breaks the balance of the GSH-mediated redox TME and enhances the sensitivity of A549 cells to cisplatin forcefully, and provides a promising way for temporal control of drug release as well as efficient cancer combination therapy.

KEYWORDS

hydrogel, programmed drug release, dual glutathione (GSH) depletion, cisplatin resistance, cancer combination therapy

1 Introduction

Cancer remains a public health challenge that poses a great threat to human health [1]. Despite today's improved cancer treatments, drug resistance continues to be unanswered as a basic question for cancer therapy [2–4]. For instance, as a first-line antitumor drug, cisplatin (cis-dichlorodiamine platinum (CDDP)) shows a broad spectrum of tumor therapeutic effects in several types of cancer [5, 6]. However, many tumors exhibit intrinsic or acquired drug resistance to cisplatin, which limits positive clinical outcomes [7]. One of the major causes of cisplatin resistance is glutathione (GSH), an important intracellular antioxidant that is overexpressed in some tumor cells and can form the GSH-Pt complex by binding with Pt [8, 9].

Combination drug therapy has become an important strategy in response to complicated tumor treatments, such as drug resistance of cancer cells [10–12]. For example, L-buthionine-sulfoximine (BSO), which can reduce the intracellular GSH concentration through inhibition of γ-glutamylcysteine synthetase (γ-GCS), has been reported to reduce cisplatin resistance and increase cisplatin-induced apoptosis [13]. Meanwhile, the strategy through GSH depletion as well as elevation of oxidative stress levels to reshape the tumor microenvironment (TME) and breakdown the intracellular antioxidant defense system has achieved exceptional tumor therapeutic effects both *in vitro* and *in vivo* [14, 15]. In addition, it has been demonstrated that regulation of payload release in controlled and programmed temporal sequences upon *in vivo* administration is important for improving cancer treatment efficacy [9, 16–18]. To date, various types of drug sequential release systems have been developed for anticancer studies [19]. Among them, engineered hydrogels have been considered promising candidates for different types of therapeutic codelivery and programmed release [20].

In this work, we developed a bioresponsive cisplatin crosslinked albumin hydrogel (BC-Gel) for sequentially delivering BSO, CDDP, and glucose (Glu) oxidase (GOx) and achieved enhanced anticancer efficiency (Scheme 1). This albumin hydrogel was formed by the coordination bonds between CDDP and the carboxyl group of bovine serum albumin (BSA), where CDDP not only was an antitumor drug but also played a cross-linking role in BC-Gel formation (Scheme 1). The small molecule drug BSO, playing a key role in blocking intracellular endogenous GSH synthesis, could be preferentially released through the three-dimensional pore structure of the hydrogel scaffold in the tumor site to sensitize the tumor cells to cisplatin against GSH-related resistance. Under the combined action of chloride ions (Cl^-) and

Address correspondence to Shuangjiang Yu, yusj@hznu.edu.cn; Shu Wei, shuwei@hznu.edu.cn

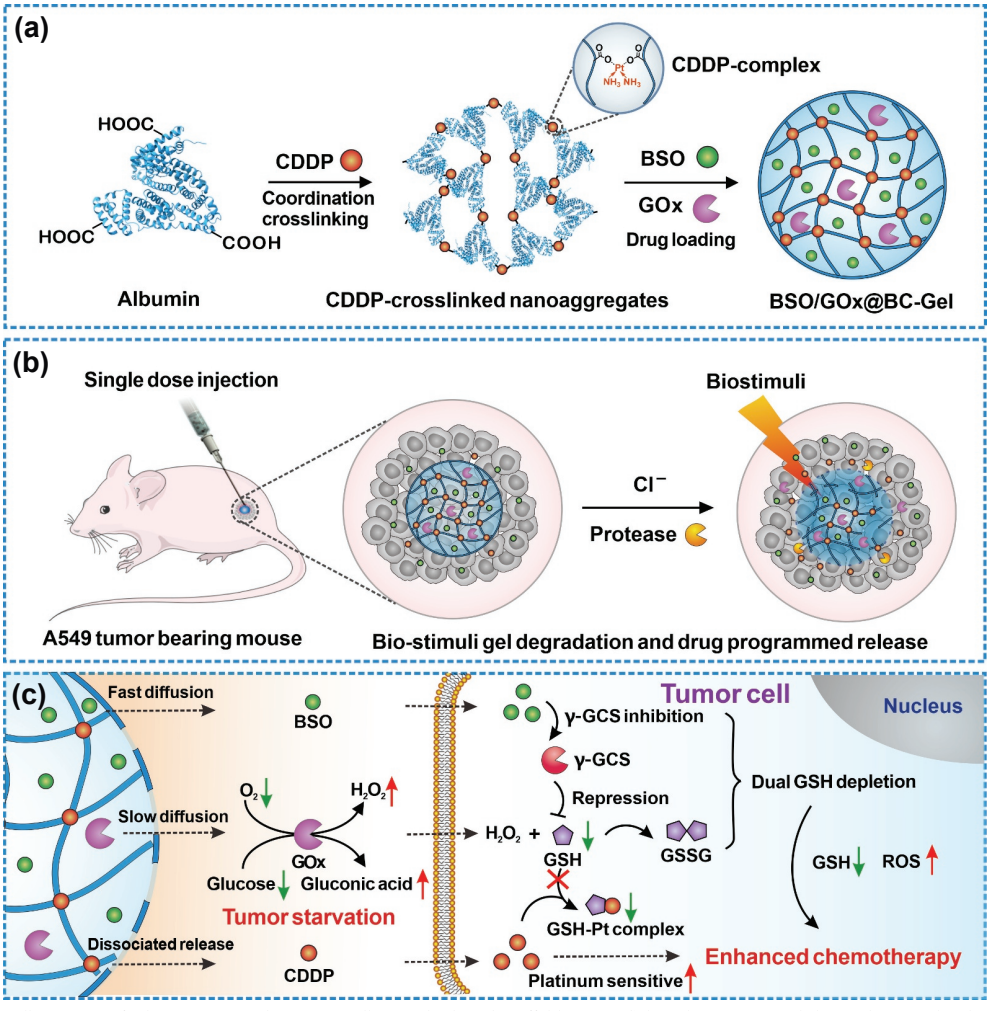

Scheme 1 Schematic illustration of a bioresponsive therapeutic albumin hydrogel scaffold (BC-Gel) based on sequential drug release and a dual GSH consumption strategy for effective antitumor therapy. (a) Preparation of the BSO and GOx coloaded hydrogel (BSO/GOx@BC-Gel). (b) Single-dose local administration of BSO/GOx@BC-Gel and programmed intratumoral drug release. (c) Mechanism of dual GSH depletion and cancer combination therapy.

enzymes in the body, cisplatin achieved sustained release following bioresponsive gel degradation (Scheme 1). Furthermore, the released GOx was involved in tumor starvation by catalyzing intratumoral glucose and O_2 transfer into gluconic acid and hydrogen peroxide (H_2O_2). The generated H_2O_2 not only accelerated the depletion of the existing intracellular GSH and further increased the sensitivity of tumor cells to cisplatin but also directly killed the tumor cells with disrupted intracellular antioxidant defenses (Scheme 1).

The above sequential drug release strategy based on the dual GSH depletion effect breaks the balance of the GSH-mediated redox TME and strongly enhances the sensitivity of tumor cells to cisplatin. This strategy achieves effective tumor regression through combined sensitized chemotherapy and starvation therapy in the following detailed study.

2 Materials and methods

2.1 Materials

Bovine serum albumin (purity 98%, sealed in dry, 2–8 °C) was purchased from Shanghai Bide Pharmatech Ltd. (Shanghai, China). Cisplatin (molecular weight 300.05) was purchased from Kunming Gui Yan Pharmaceutical Co., Ltd. (Yunnan, China). Horseradish peroxidase (HRP), glucose oxidase (lyophilized powder, 100,000–250,000 units/g solid), DL-buthionine-(S, R)-sulfoximine, and rhodamine B were obtained from Sigma–Aldrich Co., Ltd. (Shanghai, China). 3,3',5,5'-Tetramethylbenzidine (TMB) was purchased from Energy Chemical (Shanghai, China). The Calcein AM and PI Cell Viability Assay Kit and Annexin V-FITC/PI Cell Apoptosis Kit were obtained from Beyotime Biotechnology Co., Ltd. (Shanghai, China).

2.2 Cell lines and animals

The human non-small cell lung cancer cell line (A549) and murine mammary carcinoma cell line (4T1) were purchased from Meilunbio Technology Co., Ltd. (Dalian, China) and cultured in Dulbecco's modified Eagle's medium (DMEM) containing 10% fetal bovine serum (FBS) and 1% penicillin–streptomycin under standard conditions (37 °C and 5% CO_2). Phosphate buffered solution (PBS) (0.1 M, pH = 7.4) was obtained from Biosharp, Labgic Technology Co., Ltd. (Beijing, China) and diluted to 1 × PBS (0.01 M, pH: 7.2–7.4) for experiments.

2.3 BC-Gel preparation and characterization

2.3.1 BC-Gel preparation

BSA was dissolved in ultrapure water at concentrations of 8.0 wt.%, 10.0 wt.%, and 20.0 wt.%, and cisplatin (CDDP) was then added to the solution at a final concentration of 10.0 mg/mL. After that, the mixture was put into a shaking incubator (37 °C, 200 rpm/min) until formation of the BC-Gel.

2.3.2 BSO/GOx@BC-Gel preparation

A 400 μL precursor solution of BC-Gel (8.0 wt.%) was prepared with a shaking incubator. When cisplatin was fully dissolved in

BSA solution, 0.2 mg GOx and 2.0 mg BSO were then added to the blank gel for final concentrations of 0.5 and 5.0 mg/mL, respectively. After that, the mixture was put back in the shaking incubator (37 °C, 200 rpm/min) until the formation of the BSO/GOx@BC-Gel. The loading ratios (m/m) of BSO and GOx in BSO/GOx@BC-Gel (8.0 wt.%) were 0.49% and 0.05%, respectively.

2.3.3 *Gel-forming mechanism investigation*

20 μL precursor solution (8.0 wt.%) was removed at preset time intervals during the progress of hydrogel formation and then diluted to 3.0 mL with ultrapure water. Thereafter, the size distribution of the CDDP crosslinked protein particles was investigated with the above-diluted solution by dynamic light scattering (DLS, Malvern Zetasizer-ZSE). Transmission electron microscopy (TEM) images of the aggregate morphology were also obtained on a transmission electron microscopy (HT-7700, HITACHI) at 100 kV.

2.3.4 *Turbidity characterization*

2.5 mL solution of BC-Gel (8.0 wt.%) was prepared in a glass vial, and 2.0 mL solution was taken out after shaking at different times for transmittance detection directly. The value of transmittance was recorded at 500 nm by a ultraviolet–visible (UV–vis) spectrophotometer (UV-2600, Shimadzu). After that, the solution was returned to the glass vial for further cross-linking until the next preset time point.

2.3.5 *Investigation of fluorescence intensity*

In the process of gel formation, 50 μL precursor solution was taken out from the supernatant layer of the mixed solution of BC-Gel at the selected time points respectively and diluted to 2.0 mL with ultrapure water. Then, the fluorescence intensity of this diluted solution was detected at an excitation wavelength of 283 nm. The emission wavelength was recorded from 303 to 546 nm by a fluorescence spectrophotometer (FL 6500, PerkinElmer).

2.3.6 *Scanning electron microscopy*

The microstructures of the BC-Gels (8.0 wt.%, 10.0 wt.%, and 20.0 wt.%) and 8.0 wt.% BC-Gels with concentrations of CDDP (5.0, 10.0, and 12.0 mg/mL) and drug-loaded hydrogel (8.0 wt.%) were investigated by scanning electron microscopy (SEM, S-4800, HITACHI). The element distribution (C, N, O, and Pt) of 8.0 wt.% BC-Gel was investigated by SEM/energy dispersive spectroscopy (EDS) (Sigma 500, ZEISS). The samples were dried by a freeze dryer after repaid freezing in liquid nitrogen.

2.3.7 *Rheology properties test*

The rheological properties of BC-gels at different concentrations (8.0 wt.%, 10.0 wt.%, and 20.0 wt.%) and 8.0 wt.% BC-gels at different CDDP concentrations (5.0, 10.0, and 12.0 mg/mL) were analyzed with a dynamic frequency sweep from 0.1 to 100 rad/s at a fixed strain (0.1%) on a rheometer (MCR302, Anton Paar).

2.4 Hydrogel degradation behavior and drug release *in vitro*

2.4.1 *Hydrogel degradation*

500 μL of BC-Gels (8.0 wt.% and 20.0 wt.%) were respectively prepared at the bottom of glass vials for the hydrogel degradation experiment. Ultrapure water, normal saline (NS, 0.9% NaCl), trypsin (0.04 mM), trypsin+NS, or ethylene diamine tetraacetic acid (EDTA) aqueous solution (75 mM) were used as the degradation medium (500 μL, pH = 7.4), respectively. All the samples were incubated in a shaking incubator (37 °C, 76 rpm/min). The medium was carefully removed at preset intervals and the fresh medium was added after the remaining mass of every sample was recorded at preset time intervals. The detailed methods for the measurement of the gel swelling ratio were given in the Electronic Supplementary Material (ESM).

2.4.2 *Drug release investigation*

To investigate the drug release behaviors, rhodamine B (RhB) was used to mimic the small molecule drug BSO and loaded in BC-Gel (RhB@BC-Gel, 400 μL) by the experimental method shown in Section 2.3. Then, 1.0 mL of ultrapure water, NS, or NS+trypsin (0.04 mM) was used as the drug release medium. At the designated time intervals (0–6 days), 800 μL release solution was collected and replenished with an equal volume of corresponding fresh release medium. Furthermore, the release rates of RhB and CDDP were recorded by a microplate reader (Tecan Spark) and inductively coupled plasma optical emission spectrometer (ICP-OES, ICP-5000), respectively. The standard curve of RhB was given in Fig. S9 in the ESM.

2.5 Enzymatic activity evaluation of GOx in hydrogel

BSO/GOx-loaded BC-Gels (400 μL) were formed in glass vials. Then, 400 μL of NS was added to each vial and incubated on an orbital shaker at 37 °C. At the desired interval, all the media of the sample was removed and stored at 4 °C for further analysis, and another 400 μL of fresh NS was then added to the vial. The GOx-containing release solution on the sixth day was selected for enzyme activity detection. Then, 200 μL GOx-containing solution was added to the mixture solution of HAc-NaAc buffer (pH = 4, 1.2 mL), TMB (8 mM in EtOH, 200 μL), HRP (1.0 mg/mL, 50 μL), and glucose solution (10 mM, 200 μL), and the UV absorption intensity was detected at 652 nm.

The Ghose method was used for the glucose concentration test. 100 mg of 8.0 wt.% hydrogel (BC-Gel, BSO@BC-Gel, GOx@BC-Gel, and BSO/GOx@BC-Gel) and free GOx (0.005 mg/mL) were immersed in glucose solution (1.0 mg/mL, 10.0 mL with 0.9% NaCl). All the samples were incubated in a shaking incubator (37 °C, 76 rpm/min). At the preset time points (0–12 h), the mixture of supernatant, water, and DNS reagent (1:1:3, v/v/v) was heated at 100 °C for 5 min and used for detecting UV-532 nm absorption intensity by a microplate reader after cooling. The detailed methods of the standard curve of glucose were given in Fig. S10 in the ESM. The pH of the gel-containing solution was also monitored at the same time point by a pH meter (FE 28, METTLER TOLEDO).

2.6 Hydrogel hemocompatibility test

Whole blood (1.0 mL) was collected from the orbit veins of female BALB/c nude mice and stored in 2.0 mL EP tubes containing EDTA disodium salt dihydrate (saturated solution with 0.9% NaCl, 200 μL). Whole blood was diluted with PBS (10 mM, pH = 7.4), and red blood cells (RBCs) were isolated from serum by centrifugation at 2,000 rpm for 5 min. An erythrocyte suspension was obtained by washing the RBCs with PBS three times. Then, 5.0 μL of different samples (BC-Gel, BSO@BC-Gel, GOx@BC-Gel, BSO/GOx@BC-Gel, PBS, and ultrapure water) were separately mixed with the erythrocyte suspension and incubated at 37 °C for 4 h. Thereafter, the above erythrocyte suspension was centrifuged at 3,000 rpm for 5 min, and the free hemoglobin in the supernatant was detected by the UV-540 nm absorption intensity. The hemolysis rate (HR%) was calculated by the following equation

$$HR\% = (A_{Sample} - A_{NC})/(A_{PC} - A_{NC}) \times 100\% \quad (1)$$

where A_{PC} and A_{NC} are the absorbances of both positive and negative controls, respectively.

2.7 Live/dead cell assays

Live/dead cell assays were performed with a live/dead cell assay kit according to the manufacturer's instructions. Briefly, A549 cells were seeded with 2×10^4 cells per well (8-well confocal microscopy petri dishes) with 400 μL Dulbecco's modified Eagle medium (DMEM). After incubation for 24 h, the cells were washed with PBS three times to remove unattached cells. Then, the cells were incubated with free drugs (CDDP, BSO, and GOx), BC-Gel, BSO@BC-Gel, GOx@BC-Gel, and BSO/GOx@BC-Gel for another 10 h each. The final drug concentrations of CDDP, BSO, and GOx were fixed at 25, 12.5, and 1.25 μg/mL, respectively. Finally, the cells were washed with PBS, stained following the protocol specified in the Calcein AM/PI Cell Viability Assay Kit and visualized by a confocal laser scanning microscopy (CLSM, Carl Zeiss, LSM 900). The excitation wavelengths of PI and calcein AM were 488 and 561 nm, and the emission windows were 550–700 and 450–550 nm, respectively.

2.8 Cell apoptosis analysis

Cell apoptosis was evaluated using an apoptosis detection kit according to the manufacturer's instructions. Briefly, A549 cells were seeded in 6-well plates at a density of 2×10^5 cells per well in 2.5 mL DMEM at 37 °C in a 5% CO_2 atmosphere for 24 h. After that, the cells were washed with PBS thrice to remove unattached cells. Then, the cells were incubated with the free drugs BC-Gel, BSO@BC-Gel, GOx@BC-Gel, and BSO/GOx@BC-Gel for another 24 h. The final drug concentrations of CDDP, BSO, and GOx were fixed at 20.0, 10.0, and 1.0 μg/mL, respectively. Thereafter, the culture medium was collected in 15 mL centrifuge tubes separately and mixed with the corresponding cells that remained in the six-well plates, which were digested by trypsin (0.5 mL per well for 2 min). The solutions were centrifuged for 5 min at 250*g*. Cells were then resuspended in PBS (1.0 mL), and 100 μL cell suspension was used for staining with 5.0 μL Annexin V-FITC and 10 μL PI for 30 min in the cell incubator. Data of 1×10^4 events were collected, and the fluorescence intensity of cells was analyzed by a flow cytometer (BD FACS Celesta).

2.9 Cytotoxicity test *in vitro*

The A549 and 4T1 cell lines were used to evaluate the *in vitro* cytotoxicity of the free drugs and drug-loaded gel samples by 3-(4,5-dimethylthiazol-2-yl)-2,5-diphenyltetrazolium bromide (MTT) assay. Briefly, to investigate whether BSO treatment affected the cytotoxicity of cisplatin, the above tumor cells (1×10^4 per well) were separately seeded in 96-well plates with 180 μL DMEM at 37 °C in a 5% CO_2 atmosphere for 24 h. Then, the seeded cells were pretreated with BSO (0.1 mM) for 0 and 12 h with fresh culture medium (1.0 g/L Glu). After that, CDDP at different drug concentrations (6.25–50 μg/mL) was added to the pretreated cell-seeded plates. The MTT assay was performed after incubation for another 24 h by a microplate reader at 560 nm.

To evaluate the intracellular GSH depletion behavior, A549 cells (1×10^4 per well) were separately seeded in 96-well plates with 180 μL of DMEM (1.0 g/L Glu) at 37 °C in a 5% CO_2 atmosphere for 24 h. The cells were then pretreated with BSO (0.1 mM) for 0 and 12 h with fresh culture medium. After that, GOx at different concentrations (0.025–0.2 μg/mL) was added to the pretreated cell-seeded plates. The MTT assay was performed after incubation for another 24 h by a microplate reader at 560 nm.

GSH concentrations were detected by Ellman's assay. In short, A549 cells (2×10^5 cells per well) were seeded in 6-well plates with 2.5 mL DMEM at 37 °C in a 5% CO_2 atmosphere for 24 h. Then, the cells were pretreated with BSO (0.1 mM) in the same way mentioned above for 0 or 12 h with fresh culture medium (1.0 g/L Glu). GOx aqueous solution was subsequently added, and its concentration was fixed at 0.25 μg/mL. After another 12 h of incubation, the treated cells were collected and resuspended in 300 μL PBS. Frozen-thawed repeated three times with liquid nitrogen and 37 °C water bath for cell disruption. Then, the samples were mixed with 4.0% paraformaldehyde and centrifuged at 12,000 rpm for 7 min. Finally, the absorption intensity of the mixture solution of 5,5′-dithiobis (2-nitrobenzoic acid) (DTNB) (10 mM) and the supernatant was detected at UV-412 nm by a microplate reader.

A549 cells and 4T1 cells (1×10^5 per well) were separately seeded in 12-well plates with 2.0 mL DMEM (1.0 g/L Glu) at 37 °C in a 5% CO_2 atmosphere for 24 h, and then free drugs and BSO/GOx@BC-Gel were added to the cell-seeded plates and incubated for another 72 h. The final concentrations of the drugs were fixed at 12.5 to 50 μg/mL (CDDP), 6.25 to 25 μg/mL (BSO), and 0.625 to 2.5 μg/mL (GOx). The MTT assay was performed after incubation for another 72 h.

To verify the cytotoxicity of different drug-loaded hydrogels, A549 cells and 4T1 cells (5×10^4 per well) were separately seeded in 24-well plates with 1.0 mL of DMEM (1.0 g/L Glu) at 37 °C in a 5% CO_2 atmosphere for 24 h. Culture media was then removed, followed by the addition of free drugs, BC-Gel, BSO@BC-Gel, GOx@BC-Gel, and BSO/GOx@BC-Gel. The final concentrations of CDDP, BSO, and GOx were fixed at 5.0, 2.5, and 0.25 μg/mL, respectively. The MTT assay was performed after incubation for another 72 h. Cell viability was calculated by the following equation

$$\text{Cell viability}\ (\%) = (\text{OD}_{\text{Sample}}/\text{OD}_{\text{Control}}) \times 100\% \qquad (2)$$

where $\text{OD}_{\text{Sample}}$ and $\text{OD}_{\text{Control}}$ represent the MTT signals of the sample and control wells, respectively. Each data point was measured three times.

2.10 Tumor models *in vivo*

BALB/c nude mice (female, 5–6 weeks old) were purchased from SLAC Laboratory Animal Co., Ltd. (Shanghai, China). All mouse experiments were performed according to the protocol provided by Hangzhou Normal University, and the procedure was approved by the local animal ethics committee. Briefly, 5×10^6 A549 cells suspended in 50 μL PBS were transplanted into the right flanks of the mice to prepare the xenograft tumor model. When the tumor volume reached 70–80 mm^3, the following experiments were carried out in detail.

2.11 *In vivo* gel retention and drug release test

RhB was used to simulate the small molecule drug BSO, and GOx was labeled with Cy5.5-NHS ester before being used. The RhB and Cy5.5-labeled GOx coloaded hydrogel (RhB/Cy5.5-GOx@BC-Gel) was prepared according to previously described procedures. Thereafter, a 40 μL hydrogel precursor solution containing RhB and Cy5.5-GOx was mildly administered through intratumoral injection or subcutaneous injection. Then, *in vivo* fluorescence imaging was performed at different intervals by a small animal imaging system (OPTIMA, Biospace Lab). The excitation wavelengths of RhB and Cy5.5 were fixed at 562 and 662 nm, and the emission wavelengths were 597 and 697 nm, respectively. Furthermore, to estimate the drug distribution *in vivo*, the above mice were sacrificed by cervical dislocation on day 7. The major organs (heart, liver, spleen, lung, and kidney) and tumors were collected and imaged *ex vivo* using a small animal imaging system immediately.

2.12 Antitumor evaluation *in vivo*

The A549 tumor-bearing mice were randomly divided into six groups and received a single intratumoral administration of PBS (G1), free mixed drugs (G2), BC-Gel (G3), BSO@BC-Gel (G4), GOx@BC-Gel (G5), or BSO/GOx@BC-Gel (G6) (40 μL) carefully. The doses of CDDP, BSO, and GOx were fixed at 20.0, 10.0, and 1.0 mg/kg, respectively. Tumor size and mouse body weight were monitored every two days after treatments. Tumor volume was calculated according to the following equation

$$V(\mathrm{mm}^3) = (L \times W^2)/2 \quad (3)$$

where L and W represent the length and width of the tumor, respectively. After that, the survival time of the mice was recorded for another 10 days, and the mice were judged to be dead and sacrificed by cervical dislocation when the tumor volume reached ~ 1,000 mm^3.

Tumor growth inhibition (TGI) was calculated by the following equation

$$\mathrm{TGI} = (1 - \mathrm{RTV}_{\mathrm{treatment}}/\mathrm{RTV}_{\mathrm{control}}) \times 100\% \quad (4)$$

where $\mathrm{RTV}_{\mathrm{treatment}}$ represents the relative tumor volume of groups after treatment on day 20 and $\mathrm{RTV}_{\mathrm{control}}$ represents the PBS-treated group after treatment on day 20.

After treatment, tumor tissues and major organs (heart, liver, spleen, lung, and kidney) were harvested and fixed with 4% paraformaldehyde solution, followed by histopathology analysis. Briefly, tissue sections were cut into 5.0 μm thick slices. After deparaffinization, tissue sections of tumors and major organs were stained with hematoxylin/eosin (H&E) for histological analysis. Furthermore, tumor tissue slices were also stained by the TdT-mediated dUTP nick-end labeling (TUNEL) method for detecting apoptosis and Ki-67 antibody staining for immunohistochemical analysis. The images were obtained via fluorescence microscopy.

3 Results and discussion

3.1 BC-Gel formation and properties

BSA has been widely used for drug delivery studies, partly because of its structural homology and similar chemical properties to human serum albumin (HSA) [21–23]. In particular, large amounts of free carboxyl groups on the surface of BSA provide important drug binding sites [24, 25]. In addition, studies have shown that BSA could protect and stabilize the activity of the loaded bioactive molecules to a certain extent, which further expands its application potential in the field of controlled drug release [26].

In this work, for the purpose of programmed release of drugs, we first prepared a CDDP-crosslinked albumin hydrogel (BC-Gel) via the coordination crosslinking of Pt and carboxyl groups of the BSA surface (Scheme 1(a)). The vial tilt method was used to estimate BC-Gel formation. It was found that when the CDDP concentration was fixed at 10.0 mg/mL, the precursor solution with an albumin concentration of 4.0 wt.% could not form a hydrogel from beginning to end, while the 6.0 wt.% albumin concentration group could not exist stably after gel formation with little dehydration. However, the precursor solution with albumin concentration above 8.0 wt.% could form a stable hydrogel after adequate coordination crosslinking with the same drug concentration (Fig. 1(a) and Fig. S1 in the ESM).

To explore the gelation mechanism of BC-Gel, DLS was used to monitor the coordination-induced gelation progress. The results showed that the progressive growth of CDDP-crosslinked particles ranged from 1.74 to 21.04 nm within 2 days (Fig. 1(b)). TEM images also confirmed that the size of albumin nanoaggregates gradually increased with time in the progress of gel formation (Fig. S2 in the ESM). In addition, the gradient decreased the light transmittance rate, indicating the generation of hydrophobic regions in a time-dependent manner in the gel precursor solution (Fig. 1(c) and Fig. S3 in the ESM). On the other hand, it was reported that BSA has strong endogenous fluorescence due to its structure containing tyrosine (Tyr), tryptophan (Trp), and phenylalanine (Phe) residues [27, 28]. Herein, we used fluorescence spectroscopy to monitor the fluorescence intensity changes during the gelation process of BC-Gel. As shown in Fig. 1(d), the gradually decreased fluorescence suggested that the coordination between BSA and CDDP quenched the endogenous fluorescence of BSA. While there was no significant difference between BSA powder and BC-Gel observed in Fourier transform infrared (FTIR) detection (Fig. S4 in the ESM), this may be attributed to the special structure of BSA with rich carboxyl groups (–COOH), and only a few –COOH groups were involved in the coordination with CDDP. Next, it is well known that EDTA has strong chelation with many divalent metal ions. Herein, BC-Gel also presented a rapid degradation tendency when coincubated with EDTA solution compared to the control group, which suggested that the coordination interaction between cisplatin and –COOH of albumin was the major driving force for BC-Gel formation (Fig. 1(e)). All these results indicated that BC-Gel formation was caused by coordination-induced BSA-nanogel aggregation.

Then, the rheological properties of BC-Gel with different albumin concentrations (8.0 wt.%, 10.0 wt.%, and 20.0 wt.%) were investigated in detail. The results showed that the storage modulus (G') was higher than the loss modulus (G''), which demonstrated gel formation (Fig. 1(f)) [29, 30]. These results also indicated that the strength of hydrogels was obviously enhanced along with the increased protein concentration, which was due to a higher crosslinking level in the gel (Fig. 1(f) and Fig. S5(a) in the ESM). Furthermore, it was found that changes in CDDP content had little influence on G', which might be caused by the limited solubility in water (Fig. S5(b) in the ESM).

Thereafter, the microscopic morphology of BC-Gel (8.0 wt.%) was characterized by SEM after a lyophilization process. As shown in Fig. 1(g), this hydrogel has micron-scale interconnected porous structures that are beneficial for sustained drug diffusion and release [31–33]. The mapping images clearly indicated that platinum was uniformly distributed in the three-dimensional structure of BC-Gel (8.0 wt.%) (Fig. 1(j)). Notably, further investigation indicated that the concentration of BSA was a significant influencing factor for the gelation behavior and microstructure of BC-Gel (Fig. S6 in the ESM). The BC-Gel with a concentration of 10.0 wt.% showed a denser pore structure than the BC-Gel with a concentration of 8.0 wt.%, as seen in Fig. S6(a) in the ESM, which could be explained by a higher degree of crosslinking. However, excess crosslinking resulted in an unobvious pore structure of the hydrogel (20.0 wt.%), which was not conducive to the loaded drug release (Fig. S6(b) in the ESM). Moreover, it was also found that the mesh size of the BC-Gel (8.0 wt.%) was also directly influenced by the CDDP content, which offers an opportunity to tune the release behavior of large-volume drugs (Fig. 1(g)(I) and Figs. S6(c) and S6(d) in the ESM). In addition, the SEM image showed no obvious influence on the microstructure of the BC-Gel after encapsulation of BSO and GOx, as shown in Fig. 1(g)(II).

The biodegradability of implantable hydrogels is crucial for their biomedical applications [34]. Thus, the *in vitro* degradation properties of BC-Gel were investigated under different conditions at 37 °C. As shown in Fig. 1(h), the BC-Gel (8.0 wt.%) in ultrapure

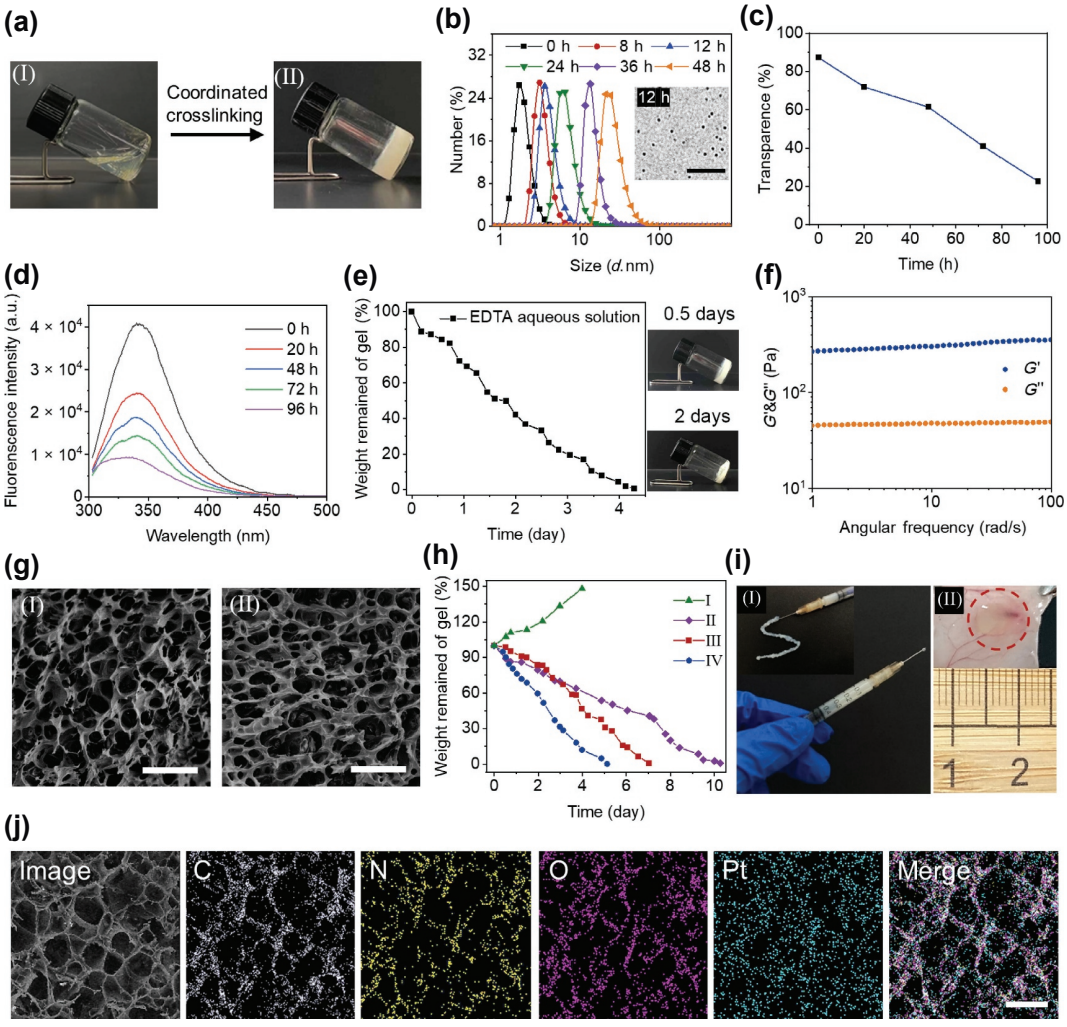

Figure 1 Formation and functional characterization of BC-Gel. (a) Photographs of the sol-to-gel transition of BC-Gel. Investigation of (b) size distribution, (c) turbidity, and (d) BSA intrinsic fluorescence intensity change during the progress of BC-Gel formation. The inset image in (b) shows a TEM image of CDDP-crosslinked albumin nanoparticles at 12 h in the progress of BC-Gel formation (scale bar: 100 nm). (e) The degradation curve of BC-Gel with EDTA aqueous solution (75 mM) at 37 °C, and the photographs show the gel degradation process. (f) The rheological properties of BC-Gel (8.0 wt.%). (g) SEM images of (I) BC-Gel and (II) BSO/GOx@BC-Gel (scale bar: 50 μm). (h) The degradation curves of BC-Gel (8.0 wt.%) at 37 °C under (I) ultrapure water, (II) NS, (III) trypsin (0.04 mM), and (IV) trypsin (0.04 mM)+NS. (i) Syringeability test of BC-Gel (I) *in vitro* and (II) *in vivo*. (j) Element mapping images of BC-Gel (8.0 wt.%) with SEM/EDS (scale bar: 50 μm).

water showed a continuous swelling tendency. The swelling rate obviously decreased with increasing albumin concentration, which likely resulted from the CDDP-induced high crosslinking degree between the intermolecular protein and protein (Fig. S7 in the ESM). Nevertheless, the BC-Gel (8.0 wt.%) in NS was almost degraded in 10 days, which might be caused by chloride ion-induced coordination-bond dissociation between cisplatin and BSA (Fig. 1(h)(II)). Similarly, the degradation rate of this gel could also be enhanced when trypsin was present in the aqueous medium (0.04 mM). Notably, BC-Gel (8.0 wt.%) exhibited the highest degradation efficiency under simulated physiological conditions (NS+trypsin) and completely degraded on day 5. Additionally, the degradation property of BC-Gel with a high albumin concentration (20.0 wt.%) was also evaluated in this work. As shown in Fig. S8 in the ESM, the results followed similar degradation trends as BC-Gel (8.0 wt.%) with a prolonged degradation time under the trypsin-presented conditions. In contrast, the NS group continued to swell during the test period, which might be due to the high intermolecular cross-linking degree of the BC-Gel. The above degradation data demonstrated that this BC-Gel had favorable biostimuli degradability features, which were advantageous for *in vivo* applications [35].

Furthermore, the injectability of pre-BC-Gel was investigated with albumin concentrations of 8.0 wt.%, 10.0 wt.%, and 20.0 wt.%. It was shown that 8.0 wt.% pre-BC-Gel can be extruded more smoothly from the 1.0 mL needle syringe and stayed in a semisolid state *in vitro* compared with the other two samples (Fig. 1(i)(I)). Meanwhile, this gel (8.0 wt.%) remained firmly under the mouse skin after subcutaneous injection, as shown in Fig. 1(i)(II). These results indicated that BC-Gel (8.0 wt.%) had good injectability *in vivo*. In view of the above investigation, BC-Gel (8.0 wt.%) was selected as a candidate for the following antitumor study.

3.2 Drug release behavior

The drug release behaviors of BC-Gel were investigated *in vitro* under different conditions. For ease of observation, RhB was used to mimic the small molecule drug BSO. As shown in Fig. 2(a), only approximately 23% of RhB was released within 6 days from BC-Gel in ultrapure water, while almost no cisplatin was released owing to restriction of Pt–O coordination bonds (Fig. 2(a)(I)). Nevertheless, nearly 60% RhB was released from the gel within 6 days, and approximately 30% CDDP was released in NS, which substantiated that the concentration of Cl^- in the body could trigger the CDDP release of BC-Gel (Fig. 2(a)(II)). Furthermore, rapid acceleration of both the CDDP and RhB release rates was

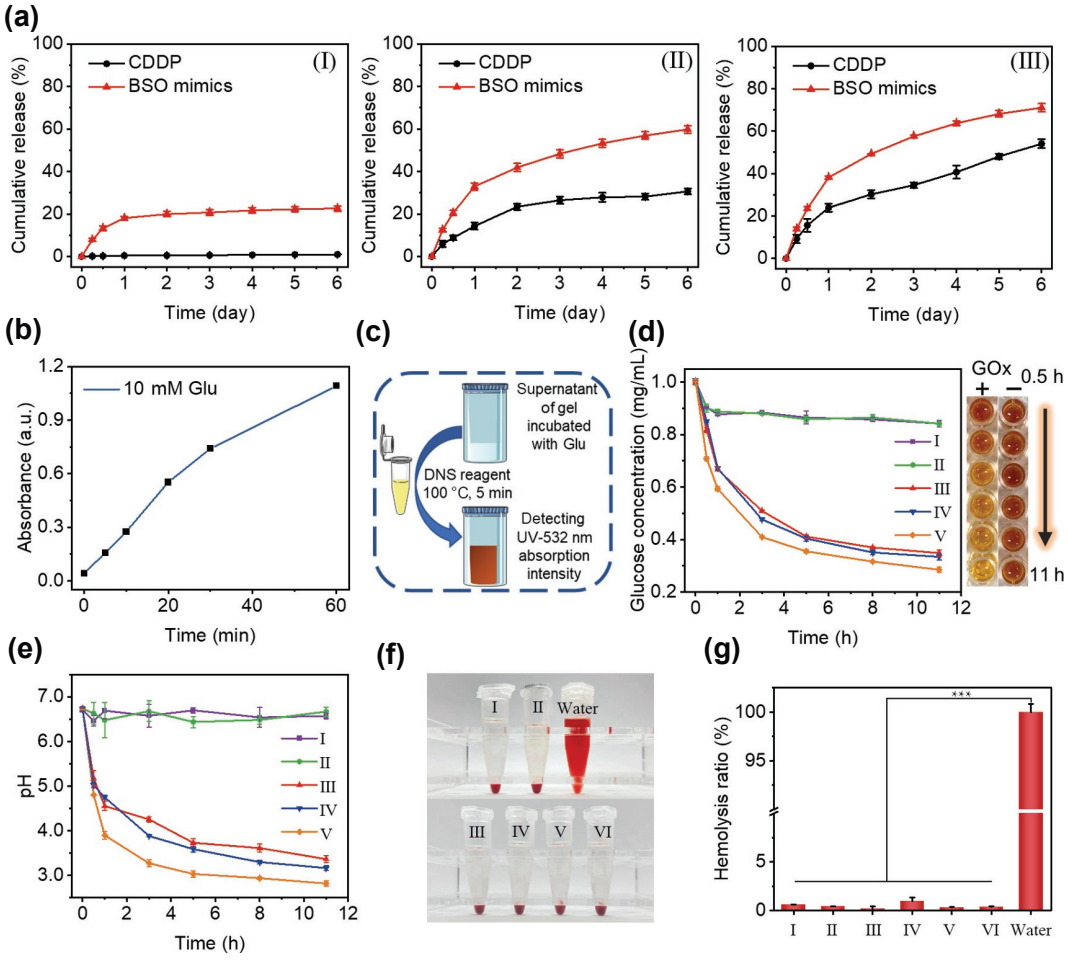

Figure 2 Drug release behaviors and blood compatibility analysis of BC-Gel (8.0 wt.%). (a) Cumulative release profiles of CDDP and RhB (BSO mimics) from RhB@BC-Gel incubated with (I) ultrapure water, (II) NS, and (III) trypsin (0.04 mM)+NS (n = 3). (b) Time-dependent UV–vis absorbance curve at 652 nm (r.t.) as a result of the catalyzed oxidation of TMB. (c) Schematic illustration of the reaction process for gel coincubation supernatant and DNS reagent by the Ghose method. Time-dependent changes in the (d) glucose concentration and (e) pH with treatments of (I) BC-Gel, (II) BSO@BC-Gel, (III) GOx@BC-Gel, (IV) BSO/GOx@BC-Gel, and (V) free drugs (CDDP+BSO+GOx) in NS. The inset image shows the color changes of treated wells incubated with blank BC-Gel (–) and GOx@BC-Gel (+) after 11 h in (d) (n = 3). (f) Digital photograph and (g) hemolysis rate (HR%) of the hemolysis test incubated with (I) PBS, (II) free drugs, (III) BC-Gel, (IV) BSO@BC-Gel, (V) GOx@BC-Gel, (VI) BSO/GOx@BC-Gel, and water (n = 3). Data are presented as the mean ± SD, and values were analyzed by one-way ANOVA with Tukey's post-hoc test; $^{*}P < 0.05$, $^{**}P < 0.01$, $^{***}P < 0.001$.

observed in the trypsin solution (0.04 mM) with 0.9% NaCl, and the cumulative release of cisplatin reached 54% within 6 days. However, the release of RhB showed a much faster release rate, which reached 57% only in the first 3 days and up to 75% on day 6 (Fig. 2(a)(III)). These data suggested that the drug release behaviors of BC-Gel could be well controlled by changing the surrounding media. Importantly, the release rate of RhB (BSO mimics) was obviously faster than that of cisplatin under the above conditions, which is consistent with our assumption. These distinct release dynamics allowed BSO and CDDP to sequentially reach the tumor microenvironment for their intended effects.

GOx is an oxidoreductase that can catalyze the oxidation of glucose to H_2O_2 and gluconic acid in the presence of O_2 and has been widely used as an antitumor agent for cancer treatment studies [36–38]. In the present system, GOx plays an important role in both promoting the tumor starvation effect and reducing the existing intracellular GSH levels. Herein, to investigate whether the encapsulation process affected GOx activity, a TMB chromogenic reaction was used to indirectly detect the enzyme activity of GOx released from BSO/GOx@BC-Gel. The results revealed that the absorbance increased gradually over time, which meant that GOx contained in the gel release solution could still effectively catalyze glucose and oxygen to produce H_2O_2, which led to the chromogenic reaction (Fig. 2(b)). Furthermore, the behaviors of both glucose consumption and pH alteration with different payload gels were determined by the Ghose method under simulated physiological conditions (1.0 mg/mL Glu with 0.9% NaCl) (Fig. 2(c)). Clearly, both BC-Gel and BSO@BC-Gel showed little influence on either glucose concentration (from 0.90 to 0.84 mg/mL) or pH when GOx was absent. Conversely, GOx-loaded GOx@BC-Gel and BSO/GOx@BC-Gel exhibited a significant reduction in glucose levels from 0.85 to 0.33 mg/mL, and the pH values were significantly reduced within 11 h (Figs. 2(d) and 2(e)). The photos also showed that the presence of GOx caused the glucose content to significantly change with gradual color deepening (Fig. 2(d)). Accordingly, the above results fully suggested that the encapsulation progress showed less effect on GOx activity, which benefited the subsequent local anticancer treatment study.

Additionally, the blood compatibility of the BC-Gel was evaluated via a hemolysis test [39]. As shown in Fig. 2(f), after 4 h of incubation at 37 °C, the supernatant displayed a bright red color in the positive control group, while all gel-containing groups showed clear supernatant. The quantitative results showed that the gel-involved groups (III–VI) had a similar hemolysis ratio as the negative control group (less than 2.0%) compared with water (Fig. 2(g)), which indicates that this BC-Gel possesses good hemocompatibility and is safe for *in vivo* biomedical applications.

3.3 *In vitro* cytotoxicity evaluation

BSO is reported to be an irreversible cell-permeable γ-GCS inhibitor of the intracellular synthesis of GSH, while GSH has been demonstrated to be one of the major causes of cisplatin resistance in tumor cells [40, 41]. Derived from this, MTT assays were performed against A549 and 4T1 cells to confirm the BSO-mediated cell sensitization to cisplatin. As shown in Fig. 3(a) and Fig. S11 in the ESM, all groups treated with BSO and CDDP simultaneously showed obviously higher cytotoxicity than the free CDDP-treated groups under different cisplatin concentrations, indicating that the BSO addition could significantly improve the sensitivity of tumor cells to CDDP. Importantly, the BSO-pretreated groups exhibited the highest cytotoxicity compared to the other experimental groups, which suggested that the BSO-pretreated cells could considerably reduce GSH-induced cisplatin resistance. Next, the combination cytotoxicity of BSO and GOx was further evaluated in the same way. The results showed that there was a positive correlation between cytotoxicity and GOx concentration. Interestingly, the BSO-pretreated groups displayed the highest cytotoxicity, which suggested that the suppression of intracellular GSH could enhance the cytotoxicity of GOx (Fig. 3(b)). Furthermore, the GSH contents in A549 tumor cells were detected by Ellman's assay after different treatments. As shown in Fig. 3(c), the intracellular GSH concentration was effectively suppressed after BSO treatment. Notably, the lowest GSH concentration was observed in the GOx+pretreated-BSO group, which strongly demonstrated the effectiveness of the dual GSH depletion.

After that, the cytotoxicity of different payload hydrogels was also investigated via MTT assays against A549 and 4T1 cells within 3 days. As shown in Fig. 3(e), for the A549 cell line, BC-Gel exhibited a certain cytotoxicity after 72 h of incubation due to the sustained release of cisplatin. Relatively, BSO/GOx@BC-Gel showed higher cytotoxicity, and the treating cell viability was fixed at 23.7%, whereas the BSO@BC-Gel and GOx@BC-Gel were 63.7% and 44.7%, respectively. Nevertheless, the free drug (CDDP, BSO, and GOx)-treated group showed the highest cytotoxicity after 72 h of incubation. Furthermore, the cytotoxicity of both the free drugs and BSO/GOx@BC-Gel exhibited an obvious drug concentration-dependent effect (Fig. 3(d)). Although these results indicated that drug-loaded BC-Gel showed a lower cytotoxic effect than free drugs due to the sustained drug release, it still caused effective tumor cell death *in vitro*. Besides, the IC_{50} values of cisplatin in BC-Gel and BSO/GOx@BC-Gel were 21.3 and 16.4 μg/mL respectively, which means that the combination treatment can effectively increase A549 cell sensitivity to cisplatin through the dual GSH-consumption effect (Fig. S12 in the ESM). Pleasingly, similar results observed in the 4T1 cell line demonstrated the universality of the above conclusion for BSO/GOx@BC-Gel (Fig. S13 in the ESM).

To further evaluate the cytotoxicity of different drug-loaded hydrogels intuitively, a cell live/dead double staining assay against the A549 cell line was performed, where live cells were stained by calcein AM with green fluorescence and dead cells were stained by PI with red fluorescence. As shown in Figs. 3(f) and 3(g), the untreated group exhibited strong green fluorescence (99.6%) as the positive control. Conversely, almost only red fluorescence (99.5%) was represented in the positive control group (free CDDP, BSO and GOx). For the groups of cells coincubated with hydrogels, no obvious red fluorescence (2.6%) was observed in BC-Gel, which might be due to the low amount of CDDP released within 10 h of incubation. Nevertheless, for BSO@BC-Gel, GOx@BC-Gel, and BSO/GOx@BC-Gel, the proportion of dead cells revealed a trend of gradual increase, 16.3%, 62.9%, and 84.6%, respectively. Similar results were further verified by flow cytometric apoptosis analysis with an Annexin V-FITC and PI double staining assay against the A549 cell line (Fig. 3(h)). The quantitative results indicated that the cell toxicity of payload gels was mainly associated with the apoptosis pathway rather than necrosis. Approximately 78.04% of cells were detected as apoptotic (Q2+Q3) after treatment with BSO/GOx@BC-Gel, which was 1.13-fold higher than GOx@BC-Gel, 1.84-fold higher than BSO@BC-Gel, and 2.6-fold higher than BC-Gel (Fig. 3(i)).

These data jointly demonstrated that BSO@BC-Gel obviously increased the sensitivity of tumor cells to cisplatin by releasing BSO preferentially from the BC-Gel. In addition, the combined use of BSO and GOx in BC-Gel inhibited the production of endogenous GSH while depleting the existing intracellular GSH level by generating H_2O_2, which further enhanced the sensitivity of cells to cisplatin, together with increasing the toxicity of residual H_2O_2 to achieve the optimal effect of tumor cell killing.

3.4 *In vivo* gel retention and drug release

The *in vivo* gel retention and drug release behaviors were evaluated against A549-bearing nude mice. To visualize the drug release behavior *in vivo*, RhB was still used as a BSO mimic, while GOx was labeled with Cy5.5-NHS ester before encapsulation in BC-Gel. Fluorescence imaging *in vivo* was performed immediately after intratumoral injection of the dye-loaded hydrogel (RhB/Cy5.5-GOx@BC-Gel). As shown in Figs. 4(a)(I) and 4(b), the fluorescence signal of Cy5.5-GOx decreased progressively and was still visible clearly on day 7 after injection, indicating that GOx was released gradually following gel degradation. On the other hand, it is suggested that this gel could be retained in mice for a long time, and 45% of the residual material remained in the tumor even on the 7th day (Fig. 4(c)). However, the fluorescent signal of RhB was barely visible on day 1 (Fig. 4(a)(II)). We presumed that the reason for this difference could be twofold. First, *in vivo* fast diffusion and metabolic processes of RhB directly caused fluorescence signal decay. Second, deep intratumoral gel administration might influence the *in vivo* fluorescence signal collection of the remaining RhB in the BC-Gel. Relatively, the fluorescence of Cy5.5-labeled GOx persisted over 7 days. This is not only because of the slower intratumoral diffusion of GOx but also due to the readily detectable Cy5.5-signals *in vivo* (RhB: ex 562 nm, em 597 nm; Cy5.5: ex 662 nm, em 697 nm) [42, 43].

To investigate the potential effect of injection depth on RhB imaging, a drug subcutaneous retention experiment was performed on BALB/c nude mice under the same conditions [44, 45]. The results showed that although the fluorescence signal of RhB decayed rapidly, it could still be detected on day 7 after subcutaneous administration, which confirmed the actual influence of the injection depth on RhB fluorescence imaging (Fig. S14 in the ESM). Nevertheless, the results revealed that Cy5.5-GOx still showed long-term retention behaviors in this process.

Additionally, the *ex vivo* images showed that there was still a strong Cy5.5 fluorescence signal but no obvious RhB fluorescence signal in the tumor tissue on day 7 (Figs. 4(d)(I) and 4(d)(II)). The data also showed that a trace fluorescence signal was detected in major organs, which may be caused by the internal metabolism of dye molecules (Fig. 4(e)). The results mentioned above confirmed that BC-Gel could serve as a local depot for the sequentially controlled release of BSO, CDDP, and GOx *in vivo*.

3.5 Antitumor efficacy *in vivo*

To evaluate the antitumor efficiency of different experimental

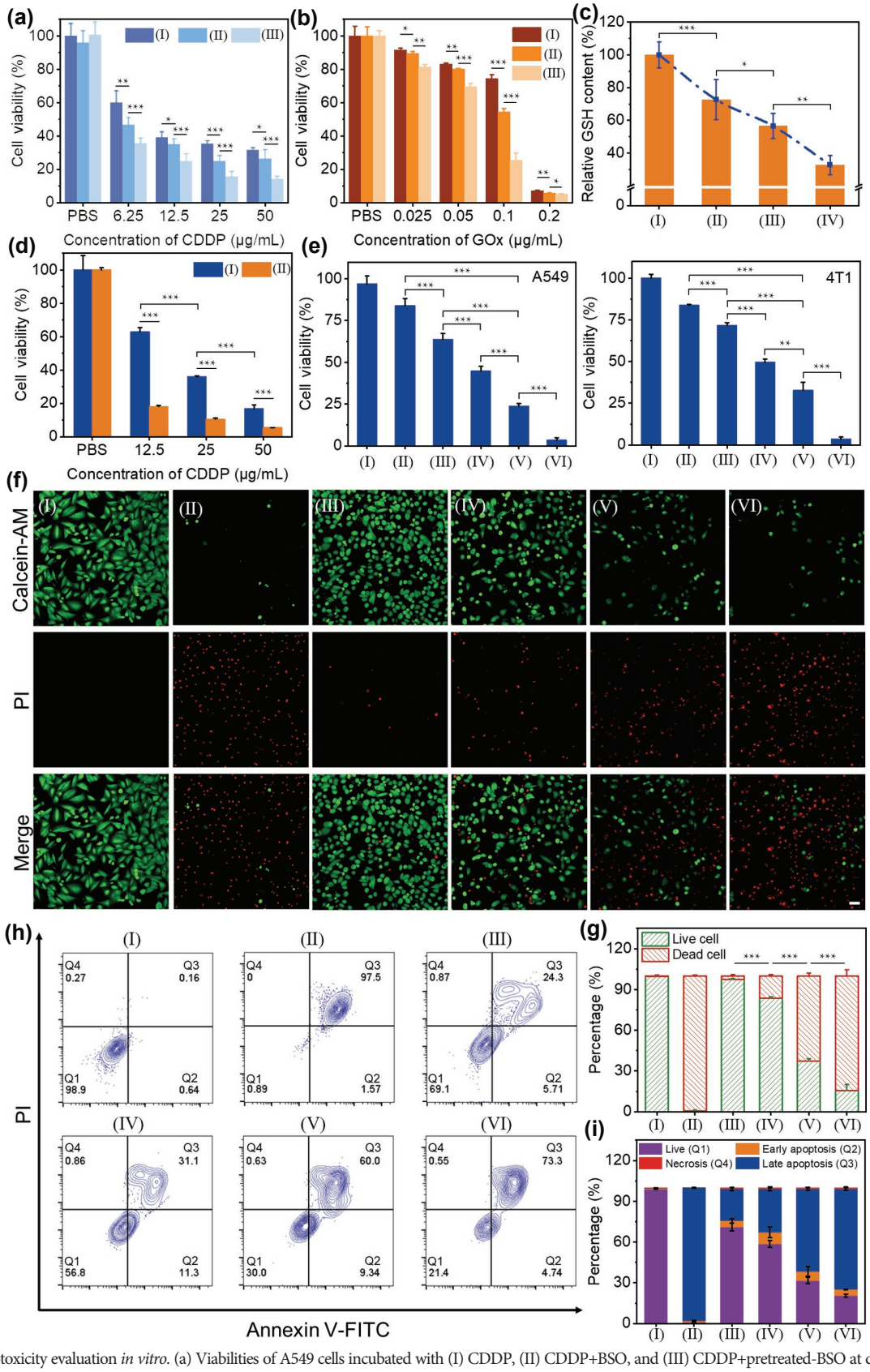

Figure 3 Cytotoxicity evaluation *in vitro*. (a) Viabilities of A549 cells incubated with (I) CDDP, (II) CDDP+BSO, and (III) CDDP+pretreated-BSO at different CDDP concentrations for 24 h ($n = 3$). (b) Viabilities of A549 cells incubated with (I) GOx, (II) GOx+BSO, and (III) GOx+pretreated-BSO at different GOx concentrations for 24 h ($n = 3$). (c) Relative GSH content of A549 cells incubated with (I) PBS, (II) BSO, (III) GOx+BSO, and (IV) GOx+pretreated-BSO for 12 h ($n = 3$). (d) Viabilities of A549 cells incubated with (I) 8.0 wt.% BSO/GOx@BC-Gel and (II) different concentrations of free CDDP, BSO, and GOx for 72 h ($n = 3$). (e) Viabilities of A549 and 4T1 cells incubated with (I) PBS, (II) BC-Gel, (III) BSO@BC-Gel, (IV) GOx@BC-Gel, (V) BSO/GOx@BC-Gel, and (VI) free drugs (CDDP+BSO+GOx) for 72 h ($n = 3$). (f) CLSM images of live/dead staining and (g) quantitative results of cell statistics after coincubation with different drug-loaded gel samples for 10 h against A549 cells. Green/red fluorescence represents living or dead cells, respectively (scale bar: 50 μm) ($n = 3$). (h) Flow cytometric apoptosis analysis and (i) statistical graph of apoptosis results of annexin V-FITC/PI-stained A549 cells after different treatments for 24 h ($n = 3$). For (f)–(i): (I) PBS, (II) free drugs (CDDP, BSO, and GOx), (III) BC-Gel, (IV) BSO@BC-Gel, (V) GOx@BC-Gel, and (VI) BSO/GOx@BC-Gel. The BSO pretreatment time was set to 12 h. Data are presented as the mean ± SD, and values were analyzed by two-tailed Student's *t*-test; $^{*}P < 0.05$, $^{**}P < 0.01$, $^{***}P < 0.001$.

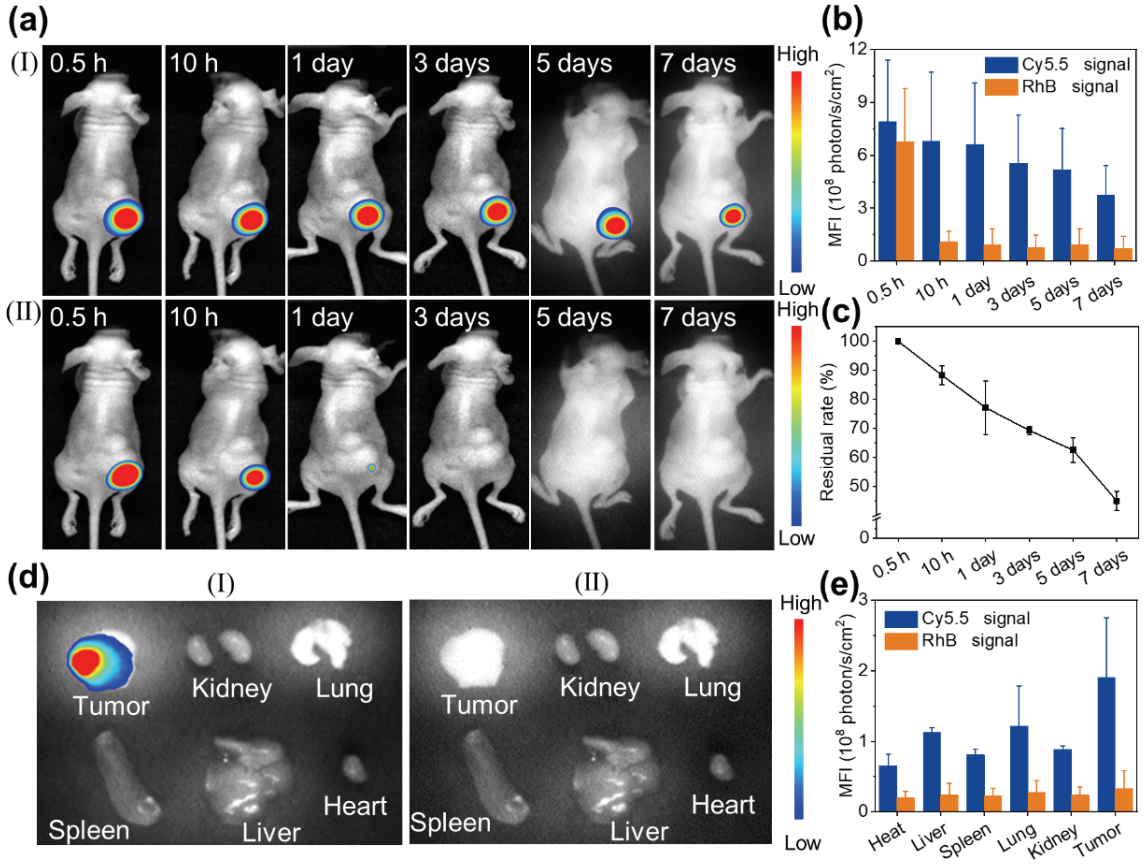

Figure 4 *In vivo* gel retention and drug release against A549 tumor-bearing nude mice. (a) Fluorescent images of (I) Cy5.5-labeled GOx and (II) RhB after receiving intratumoral treatments of RhB/Cy5.5-GOx@BC-Gel within 7 days *in vivo*. (b) Mean fluorescence intensity (MFI) of Cy5.5 and RhB (n = 3). (c) *In vivo* residual rate of gel at 0.5 h, 10 h, 1 day, 3 days, 5 days, and 7 days (n = 3). (d) *Ex vivo* tissue imaging and (e) MFI of (I) Cy5.5 and (II) RhB signals at day 7 (n = 3).

groups, A549-bearing female nude mice were randomly divided into 6 groups and treated with a single intratumoral injection of PBS (G1), free drugs (BSO, CDDP and GOx) (G2), BC-Gel (G3), BSO@BC-Gel (G4), GOx@BC-Gel (G5), or BSO/GOx@BC-Gel (G6) when the tumor volumes reached ~ 80 mm^3 on the 7th day (Fig. 5(a)). In the following 20 days, tumor growth and mouse body weight were monitored every two days (Fig. 5). It was shown that the tumor growth of all of the treatment groups (G2–G6) was inhibited to some degree compared to the PBS-treated group (G1). As shown in Figs. 5(b) and 5(c), the free drug-treated group (G2) exhibited significant tumor inhibition within the first five days after administration, but then the tumor grew out of control. This result might be caused by the rapid diffusion and metabolism of free drugs *in vivo*, which could not meet the effective drug dose after being treated for 5 days. Furthermore, the final TGI rate of G2 was only 5.5% compared to that of the control group, suggesting that the free drug treatment group maintained little antitumor efficiency after 20 days of treatment (Fig. 5(d)). In contrast, all gel-treated groups (G3–G6) showed different degrees of inhibition of tumor growth, and the TGIs of G3 to G5 were fixed at 17.0%, 38.6%, and 61.8%, respectively, on day 20, owing to the long-acting retention and the sustained drug release properties of BC-Gel. Encouragingly, the tumor growth of the mice treated with BSO/GOx@BC-Gel (G6) was distinctly suppressed compared with those of the other five groups (G1–G5), with the highest TGI value at 96.0% (Figs. 5(d) and 5(e)). During the treatment, all mice in the drug treatment group (G2–G6) showed a slight decrease in body weight within two days after treatment, followed by a gradual increase over time, which suggested the good safety of this treatment strategy (Fig. 5(f)). Additionally, the mouse survival rate of G6 was obviously prolonged compared to that of the other five experimental groups within the observed 30 days (Fig. 5(g)).

To further investigate the antitumor efficacy of the albumin hydrogels, the tumor tissues and major organs were preserved for histomorphological staining and immunohistochemical analysis at the 20th day posttreatment (Fig. 6(a)). It was suggested that the tumor treated with BSO/GOx@BC-Gel (G6) had the sparsest nuclei (stained by deep purple) in H&E staining compared with other groups (G1-G5), demonstrating that the drug coloaded gel caused the most severe cell damage as well as necrosis in tumor tissue. Furthermore, the results of the TUNEL assay clearly revealed that the tumor tissue sections from G1 to G6 exhibited increasing red fluorescence, which confirmed once more that the BSO and GOx combined therapy group (G6) could induce most tumor cell apoptosis effectively. Additionally, similar results were further confirmed in the Ki-67 immunohistochemical staining images. It could be observed that the PBS-treated group (G1) showed a large number of Ki-67-positive proliferating cells (stained by brown), while the drug-loaded gel-treated group (G6) was in stark contrast that performed the lowest extent of cell proliferation level among all positive control groups (G2–G5). The H&E staining images of the main organs, including the heart, liver, spleen, lung, and kidney, showed a normal, defect-free organizational structure without hemorrhage and inflammatory infiltration, which also proved that the BC-Gel-based drug delivery system had good systemic safety (Fig. 6(b) and Fig. S15 in the ESM).

Collectively, these results are consistent with the tumor suppression results mentioned above, indicating that this hydrogel drug delivery system can effectively inhibit tumor proliferation and promote tumor cell apoptosis through local treatment with favorable biosafety.

4 Conclusions

In summary, we have generated a new bioresponsive therapeutic

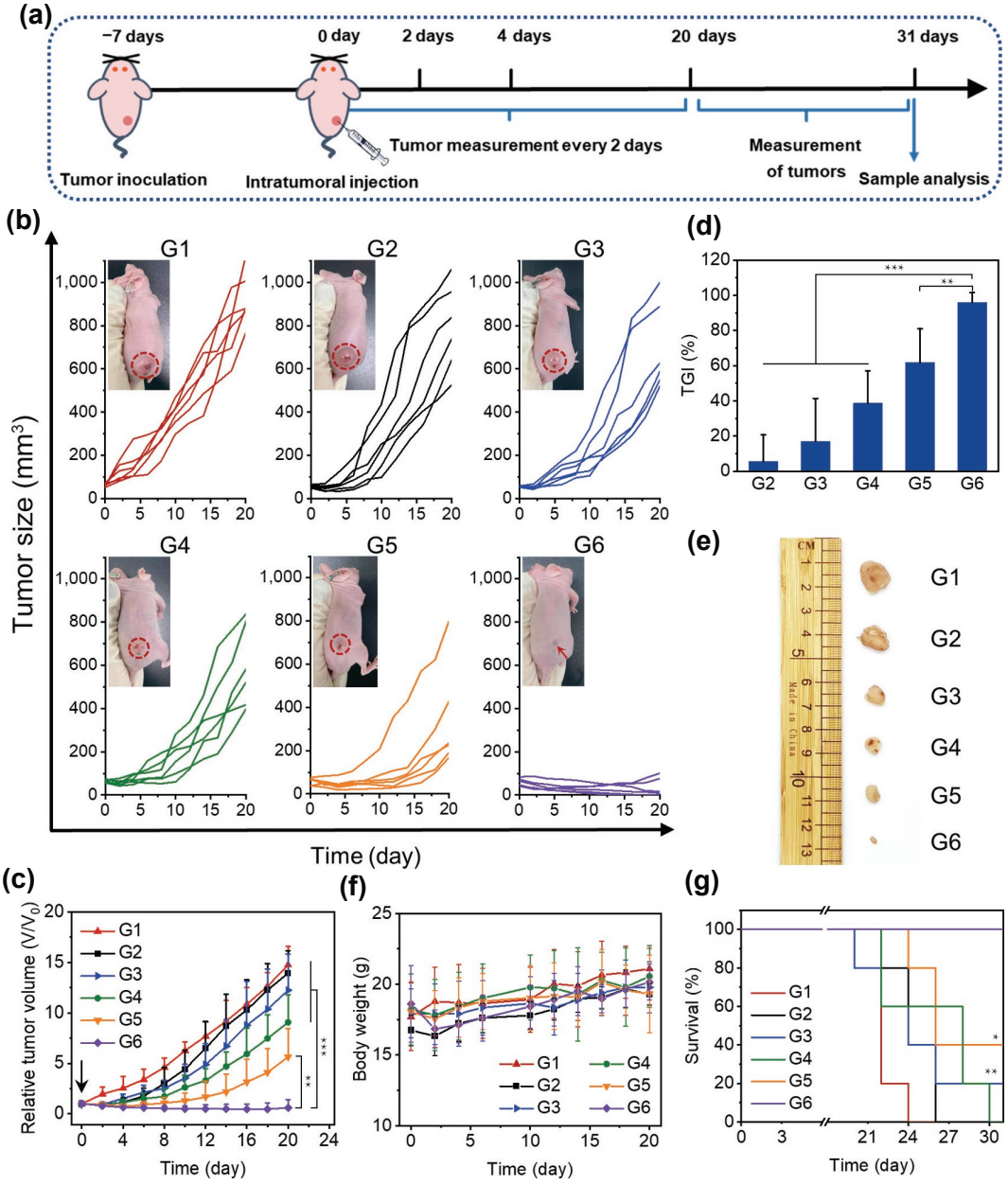

Figure 5 *In vivo* antitumor efficacy evaluation against A549 tumor-bearing nude mice. (a) Experimental design and timeline for BC-Gel-involved antitumor treatments. (b) Quantified individual tumor growth curves and (c) RTV of mice with different treatments within 20 days (n = 6). Representative photographs (inset) show the therapeutic results of mice 20 days posttreatment. ((b): The dotted red lines indicate the location of tumors, and the red arrow represents a mouse that was completely cured in G6; (c): the black arrow represents single-dose local administration.) (d) TGI rate and (e) typical tumor photographs after various treatments (n = 6). (f) Mouse body weights of different groups during the treatment (n = 6). (g) Survival rates of mice after different treatments for 30 days (n = 5). G1: PBS, G2: free drugs (CDDP, BSO, and GOx), G3: BC-Gel, G4: BSO@BC-Gel, G5: GOx@BC-Gel, G6: BSO/GOx@BC-Gel. (The doses of CDDP, BSO, and GOx were fixed at 20.0, 10.0, and 1.0 mg/kg, respectively.) Data are presented as the mean ± SD, and values were analyzed by one-way ANOVA with Tukey's post-hoc test; $^{*}P < 0.05$, $^{**}P < 0.01$, $^{***}P < 0.001$.

albumin hydrogel based on the coordination reaction between cisplatin and BSA for combination cancer therapy that pertinently depleted intracellular GSH and sensitized tumor cells to cisplatin. This drug-crosslinked protein gel not only showed favorable biostimuli degradability and injectability but also could sequentially deliver BSO, CDDP, and GOx with different release kinetics *in situ*. The *in vivo* study demonstrated that the BSO/GOx@BC-Gel could obviously enhance the antitumor efficacy through the combined sensitized chemotherapy and starvation therapy compared to the free drugs at a comparable dose. Inconspicuous toxicity to normal organs indicated the excellent biocompatibility of the albumin hydrogel-based drug delivery system. Taken together, this novel therapeutic strategy paves a promising way for not only temporal control of drugs but also multidrug combination in efficient cancer therapy.

Acknowledgments

This work was supported by the National Natural Science Foundation of China (Nos. 22075065, 22161142015, and 22001054), the National Key R&D Program of China (Nos. 2020YFA0908500 and 2018YFA0901600), and the Research Start-up Fund from Hangzhou Normal University (Nos. 2019QDL025, 2019QDL026, and 4095C5022121604).

Electronic Supplementary Material: Supplementary material (further details of photos, rheological properties measurement, SEM, TEM, degradation experiment, swelling test for different proportions of BC-Gels, results about transmittance test, FTIR, standard curves, fluorescence imaging experiments *in vivo*, MTT assays of 4T1 and H&E staining of major organs) is available in

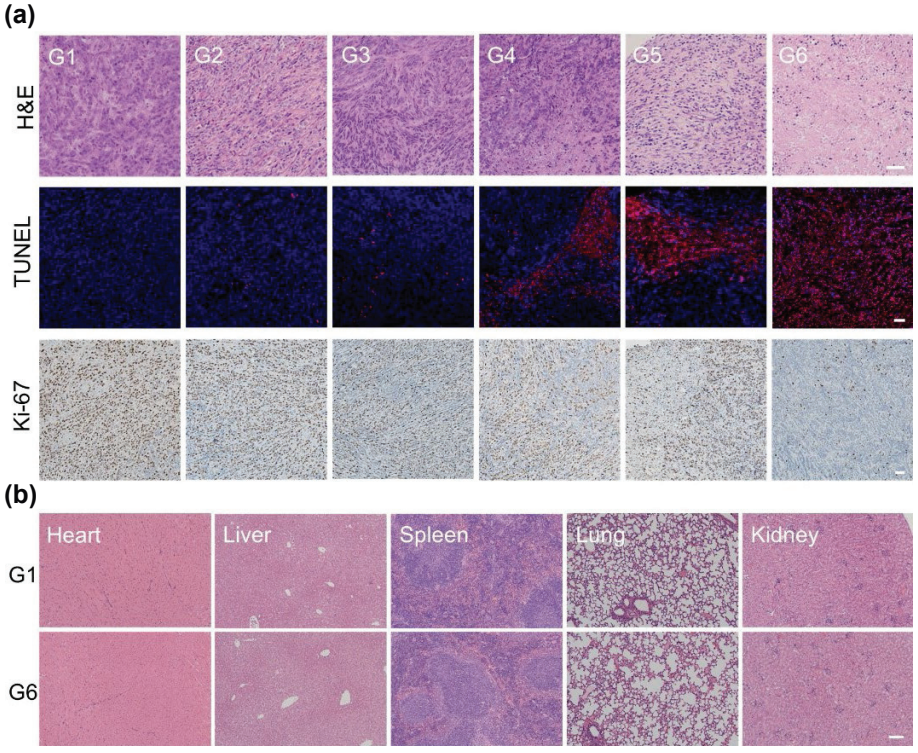

Figure 6 Pathological investigation after treatment with various treatments. (a) *Ex vivo* H&E histomorphological staining, TUNEL assay, and Ki-67 immunohistochemical staining of A549 tumor tissues after single-dose treatments with various therapeutics after 20 days (scale bar: 50 μm). (b) Representative H&E staining images of major organs (heart, liver, spleen, lung, and kidney) 20 days posttreatment (scale bar: 100 μm). G1: PBS, G2: free drugs (CDDP, BSO, and GOx), G3: BC-Gel, G4: BSO@BC-Gel, G5: GOx@BC-Gel, G6: BSO/GOx@BC-Gel.

the online version of this article at http://doi.org/10.1007/s12274-022-4925-y.

References

[1] Mao, J. J.; Pillai, G. G.; Andrade, C. J.; Ligibel, J. A.; Basu, P.; Cohen, L.; Khan, I. A.; Mustian, K. M.; Puthiyedath, R.; Dhiman, K. S. et al. Integrative oncology: Addressing the global challenges of cancer prevention and treatment. *CA A Cancer J. Clin.* **2022**, *72*, 144–164.

[2] Bourzac, K. Biology: Three known unknowns. *Nature* **2014**, *509*, S69–S71.

[3] Ward, R. A.; Fawell, S.; Floc'h, N.; Flemington, V.; McKerrecher, D.; Smith, P. D. Challenges and opportunities in cancer drug resistance. *Chem. Rev.* **2021**, *121*, 3297–3351.

[4] Ma, W.; Chen, Q. L.; Xu, W. G.; Yu, M.; Yang, Y. Y.; Zou, B. H.; Zhang, Y. S.; Ding, J. X.; Yu, Z. Q. Self-targeting visualizable hyaluronate nanogel for synchronized intracellular release of doxorubicin and cisplatin in combating multidrug-resistant breast cancer. *Nano Res.* **2021**, *14*, 846–857.

[5] Liu, C. F.; Zhou, S. J.; Bai, W. B.; Shi, L.; Li, X. L. Protective effect of food derived nutrients on cisplatin nephrotoxicity and its mechanism. *Food Funct.* **2022**, *13*, 4839–4860.

[6] He, S. S.; Li, C.; Zhang, Q. F.; Ding, J. X.; Liang, X. J.; Chen, X. S.; Xiao, H. H.; Chen, X. Y.; Zhou, D. F.; Huang, Y. B. Tailoring Platinum(IV) amphiphiles for self-targeting all-in-one assemblies as precise multimodal theranostic nanomedicine. *ACS Nano* **2018**, *12*, 7272–7281.

[7] Rottenberg, S.; Disler, C.; Perego, P. The rediscovery of platinum-based cancer therapy. *Nat. Rev. Cancer* **2021**, *21*, 37–50.

[8] Li, S. Y.; Li, C.; Jin, S. B.; Liu, J.; Xue, X. D.; Eltahan, A. S.; Sun, J. D.; Tan, J. J.; Dong, J. C.; Liang, X. J. Overcoming resistance to cisplatin by inhibition of glutathione S-transferases (GSTs) with ethacraplatin micelles *in vitro* and *in vivo*. *Biomaterials* **2017**, *144*, 119–129.

[9] Shi, F. H.; Ding, J. X.; Xiao, C. S.; Zhuang, X. L.; He, C. L.; Chen, L.; Chen, X. S. Intracellular microenvironment responsive PEGylated polypeptide nanogels with ionizable cores for efficient doxorubicin loading and triggered release. *J. Mater. Chem.* **2012**, *22*, 14168–14179.

[10] Lv, Q.; Yu, S. J.; Quan, F. L.; He, C. L.; Chen, X. S. Thermosensitive polypeptide hydrogels Co-loaded with two anti-tumor agents to reduce multi-drug resistance and enhance local tumor treatment. *Adv. Therap.* **2020**, *3*, 1900165.

[11] Liu, J. F.; Gefen, O.; Ronin, I.; Bar-Meir, M.; Balaban, N. Q. Effect of tolerance on the evolution of antibiotic resistance under drug combinations. *Science* **2020**, *367*, 200–204.

[12] Jiang, L.; Ding, Y.; Xue, X. L.; Zhou, S. S.; Li, C.; Zhang, X. K.; Jiang, X. Q. Entrapping multifunctional dendritic nanoparticles into a hydrogel for local therapeutic delivery and synergetic immunochemotherapy. *Nano Res.* **2018**, *11*, 6062–6073.

[13] Wang, W. M.; Kryczek, I.; Dostál, L.; Lin, H.; Tan, L. J.; Zhao, L. L.; Lu, F. J.; Wei, S.; Maj, T.; Peng, D. J. et al. Effector T cells abrogate stroma-mediated chemoresistance in ovarian cancer. *Cell* **2016**, *165*, 1092–1105.

[14] Wu, F.; Du, Y. Q.; Yang, J. N.; Shao, B. Y.; Mi, Z. S.; Yao, Y. F.; Cui, Y.; He, F.; Zhang, Y. Q.; Yang, P. P. Peroxidase-like active nanomedicine with dual glutathione depletion property to restore oxaliplatin chemosensitivity and promote programmed cell death. *ACS Nano* **2022**, *16*, 3647–3663.

[15] Lu, S. C. Regulation of glutathione synthesis. *Mol. Aspects Med.* **2009**, *30*, 42–59.

[16] Dong, Z. L.; Feng, L. Z.; Hao, Y.; Li, Q. G.; Chen, M. C.; Yang, Z. J.; Zhao, H.; Liu, Z. Synthesis of $CaCO_3$-based nanomedicine for enhanced sonodynamic therapy via amplification of tumor oxidative stress. *Chem* **2020**, *6*, 1391–1407.

[17] Li, Z. M.; Xu, W. G.; Yang, J. Z.; Wang, J.; Wang, J. L.; Zhu, G.; Li, D.; Ding, J. X.; Sun, T. M. A tumor microenvironments-adapted polypeptide hydrogel/nanogel composite boosts antitumor molecularly targeted inhibition and immunoactivation. *Adv. Mater.* **2022**, *34*, 2200449.

[18] Lang, T. Q.; Liu, Y. R.; Zheng, Z.; Ran, W.; Zhai, Y. H.; Yin, Q.; Zhang, P. C.; Li, Y. P. Cocktail strategy based on spatio-temporally controlled nano device improves therapy of breast cancer. *Adv. Mater.* **2019**, *31*, 1806202.

[19] Ahmadi, S.; Rabiee, N.; Bagherzadeh, M.; Elmi, F.; Fatahi, Y.;

Farjadian, F.; Baheiraei, N.; Nasseri, B.; Rabiee, M.; Dastjerd, N. T. et al. Stimulus-responsive sequential release systems for drug and gene delivery. *Nano Today* **2020**, *34*, 100914.

[20] Wang, C.; Wang, J. Q.; Zhang, X. D.; Yu, S. J.; Wen, D.; Hu, Q. Y.; Ye, Y. Q.; Bomba, H.; Hu, X. L.; Liu, Z. et al. *In situ* formed reactive oxygen species-responsive scaffold with gemcitabine and checkpoint inhibitor for combination therapy. *Sci. Transl. Med.* **2018**, *10*, eaan3682.

[21] An, F. F.; Zhang, X. H. Strategies for preparing albumin-based nanoparticles for multifunctional bioimaging and drug delivery. *Theranostics* **2017**, *7*, 3667–3689.

[22] Hoogenboezem, E. N.; Duvall, C. L. Harnessing albumin as a carrier for cancer therapies. *Adv. Drug Deliv. Rev.* **2018**, *130*, 73–89.

[23] Chen, Q.; Feng, L. Z.; Liu, J. J.; Zhu, W. W.; Dong, Z. L.; Wu, Y. F.; Liu, Z. Intelligent albumin-MnO_2 nanoparticles as pH-/H_2O_2-responsive dissociable nanocarriers to modulate tumor hypoxia for effective combination therapy. *Adv. Mater.* **2016**, *28*, 7129–7136.

[24] Karimi, M.; Bahrami, S.; Ravari, S. B.; Zangabad, P. S.; Mirshekari, H.; Bozorgomid, M.; Shahreza, S.; Sori, M.; Hamblin, M. R. Albumin nanostructures as advanced drug delivery systems. *Expert Opin. Drug Deliv.* **2016**, *13*, 1609–1623.

[25] Elzoghby, A. O.; Samy, W. M.; Elgindy, N. A. Albumin-based nanoparticles as potential controlled release drug delivery systems. *J. Control. Release* **2012**, *157*, 168–182.

[26] He, C. X.; Liu, J. H.; Xie, L. Y.; Zhang, Q. L.; Li, C. H.; Gui, D. Y.; Zhang, G. Z.; Wu, C. Activity and thermal stability improvements of glucose oxidase upon adsorption on core−shell PMMA-BSA nanoparticles. *Langmuir* **2009**, *25*, 13456–13460.

[27] Kiraz, S.; İnci, D.; Aydın, R.; Vatan, Ö.; Zorlu, Y.; Cavaş, T. Antiproliferative activity of copper(II) glutamine complexes with *N, N*-donor ligands: Synthesis, characterization, potentiometric studies and DNA/BSA interactions. *J. Mol. Struct.* **2019**, *1194*, 245–255.

[28] Li, J. B.; Wang, X. Y. Binding of (–)-epigallocatechin-3-gallate with thermally-induced bovine serum albumin/ι-carrageenan particles. *Food Chem.* **2015**, *168*, 566–571.

[29] Xing, R. R.; Liu, K.; Jiao, T. F.; Zhang, N.; Ma, K.; Zhang, R. Y.; Zou, Q. L.; Ma, G. H.; Yan, X. H. An injectable self-assembling collagen-gold hybrid hydrogel for combinatorial antitumor photothermal/photodynamic therapy. *Adv. Mater.* **2016**, *28*, 3669–3676.

[30] Catoira, M. C.; Fusaro, L.; Di Francesco, D.; Ramella, M.; Boccafoschi, F. Overview of natural hydrogels for regenerative medicine applications. *J. Mater. Sci. Mater. Med.* **2019**, *30*, 115.

[31] Seliktar, D. Designing cell-compatible hydrogels for biomedical applications. *Science* **2012**, *336*, 1124–1128.

[32] Cui, C. Y.; Liu, W. G. Recent advances in wet adhesives: Adhesion mechanism, design principle and applications. *Prog. Polym. Sci.* **2021**, *116*, 101388.

[33] Chen, Q.; Wang, C.; Zhang, X. Q.; Chen, G. J.; Hu, Q. Y.; Li, H. J.; Wang, J. Q.; Wen, D.; Zhang, Y. Q.; Lu, Y. F. et al. *In situ* sprayed bioresponsive immunotherapeutic gel for post-surgical cancer treatment. *Nat. Nanotechnol.* **2019**, *14*, 89–97.

[34] Li, Y.; Yang, H. Y.; Lee, D. S. Advances in biodegradable and injectable hydrogels for biomedical applications. *J. Controlled Release* **2021**, *330*, 151–160.

[35] Norouzi, M.; Nazari, B.; Miller, D. W. Injectable hydrogel-based drug delivery systems for local cancer therapy. *Drug Discov. Today* **2016**, *21*, 1835–1849.

[36] Yu, S. J.; Chen, Z. W.; Zeng, X.; Chen, X. S.; Gu, Z. Advances in nanomedicine for cancer starvation therapy. *Theranostics* **2019**, *9*, 8026–8047.

[37] Li, C. Y.; Wan, Y. L.; Zhang, Y. F.; Fu, L. H.; Blum, N. T.; Cui, R.; Wu, B. D.; Zheng, R.; Lin, J.; Li, Z. M. et al. *In situ* sprayed starvation/chemodynamic therapeutic gel for post-surgical treatment of IDH1 (R132H) Glioma. *Adv. Mater.* **2022**, *34*, 2103980.

[38] He, X. L.; Hao, Y.; Chu, B. Y.; Yang, Y.; Sun, A.; Shi, K.; Yang, C. L.; Zhou, K.; Qu, Y.; Li, H. et al. Redox-activatable photothermal therapy and enzyme-mediated tumor starvation for synergistic cancer therapy. *Nano Today* **2021**, *39*, 101174.

[39] Wang, M.; Chen, M.; Niu, W.; Winston, D. D.; Cheng, W.; Lei, B. Injectable biodegradation-visual self-healing citrate hydrogel with high tissue penetration for microenvironment-responsive degradation and local tumor therapy. *Biomaterials* **2020**, *261*, 120301.

[40] Niu, B. Y.; Liao, K. X.; Zhou, Y. X.; Wen, T.; Quan, G. L.; Pan, X.; Wu, C. B. Application of glutathione depletion in cancer therapy: Enhanced ROS-based therapy, ferroptosis, and chemotherapy. *Biomaterials* **2021**, *277*, 121110.

[41] Yu, J.; Xiao, H.; Yang, Z.; Qiao, C. Q.; Zhou, B.; Jia, Q.; Wang, Z. D.; Wang, X. F.; Zhang, R. L.; Yang, Y. et al. A potent strategy of combinational blow toward enhanced cancer chemo-photodynamic therapy via sustainable GSH elimination. *Small* **2022**, *18*, 2106100.

[42] Barbosa, R. I.; Guirro, E. C. D. O.; Bachmann, L.; Brandino, H. E.; Guirro, R. R. D. J. Analysis of low-level laser transmission at wavelengths 660, 830 and 904 nm in biological tissue samples. *J. Photochem. Photobiol. B Biol.* **2020**, *209*, 111914.

[43] Salehpour, F.; Cassano, P.; Rouhi, N.; Hamblin, M. R.; De Taboada, L.; Farajdokht, F.; Mahmoudi, J. Penetration profiles of visible and near-infrared lasers and light-emitting diode light through the head tissues in animal and human species: A review of literature. *Photobiomodul. Photomed. Laser Surg.* **2019**, *37*, 581–595.

[44] Kolárová, H.; Ditrichová, D.; Wagner, J. Penetration of the laser light into the skin *in vitro*. *Lasers Surg. Med.* **1999**, *24*, 231–235.

[45] Joensen, J.; Øvsthus, K.; Reed, R. K.; Hummelsund, S.; Iversen, V. V.; Lopes-Martins, R. Á.; Bjordal, J. M. Skin penetration time-profiles for continuous 810 nm and Superpulsed 904 nm lasers in a rat model. *Photomed. Laser Surg.* **2012**, *30*, 688–694.